plasma

MDPI

Article

Spatially Resolved Inactivation of *Escherichia coli* in a RF (13.56 MHz) Capacitively Coupled Air Plasma at 4.0 mbar

Mahmood Nasser [1,*], Layla Nasser [1], Fatima Makhlooq [1], Batool Abulwahab [2] and Elias Naser [3]

[1] Department of Physics, University of Bahrain, Zallaq P.O. Box 32038, Bahrain; lsaleh@uob.edu.bh (L.N.)
[2] Department of Biology, University of Bahrain, Zallaq P.O. Box 32038, Bahrain; bahmed@uob.edu.bh
[3] Salmaniya Medical Complex (SMC), Manama P.O. Box 12, Bahrain
* Correspondence: snasser@uob.edu.bh

Abstract

A spatially resolved investigation of bacterial inactivation using a radiofrequency (13.56 MHz) capacitively coupled plasma (RF CCP) discharge operating in ambient air at 4.0 mbar is presented. The plasma was generated in a parallel-plate reactor without external gas precursors and characterized using Langmuir probe diagnostics and optical emission spectroscopy (OES). Electron densities on the order of 109 cm^3 were measured near the powered electrode, exhibiting pronounced axial and radial gradients across the discharge volume. OES revealed strong excitation of oxygen- and nitrogen-containing emitters, including O I (777 nm), N_2 s positive system (337–380 nm), and N_2^+ first negative system features, with emission intensities increasing monotonically with applied RF power. The bactericidal performance was evaluated using *Escherichia coli* American Type Culture Collection (ATCC) 11775 exposed at different axial and radial positions within the reactor. At a fixed exposure time of 60 s, the $\log_{10}$ reduction increased nonlinearly with RF power, rising from 0.29 at 20 W to 0.81 at 40 W, followed by a sharp transition to the assay reporting ceiling ($\geq$2.95-$\log_{10}$ under the adopted half-count correction) at 50 W and above. Time-resolved measurements at 50 W demonstrated rapid inactivation kinetics, with measurable reductions occurring within 5–10 s and reaching the reporting ceiling within 60 s. In contrast, samples positioned at the chamber periphery or approximately 20 cm from the discharge center exhibited negligible inactivation, confirming strong spatial localization of the biocidal effect. These results identify a threshold-like operating regime in which increased discharge intensity produces rapid inactivation in the plasma core while remaining strongly position dependent. The findings establish medium pressure, air-based RF CCP as an efficient, gas-free, and spatially controllable platform for localized surface decontamination under non-thermal conditions.

Keywords: plasma inactivation; RF capacitively coupled plasma; *Escherichia coli*; Langmuir probe; optical emission spectroscopy; air plasma

Check for updates

Academic Editor: Andrey Starikovskiy

Received: 10 March 2026
Revised: 20 March 2026
Accepted: 27 March 2026
Published: 31 March 2026

Copyright: © 2026 by the authors. Licensee MDPI, Basel, Switzerland. This article is an open access article distributed under the terms and conditions of the Creative Commons Attribution (CC BY) license.

1. Introduction

Non-thermal plasma (NTP) has emerged as a powerful and versatile technology for microbial inactivation in biomedical sterilization, food safety, and environmental decontamination applications [1,2]. Unlike conventional thermal or chemical sterilization methods, NTP operates at near-ambient temperatures while generating a rich mixture of reactive oxygen and nitrogen species (RONS), ultraviolet (UV) radiation, charged particles, and metastable species capable of efficiently inactivating microorganisms without damaging

heat-sensitive materials [2,3]. These unique features make plasma-based sterilization an attractive alternative to traditional approaches that rely on elevated temperatures or toxic chemical disinfectants.

Microbial inactivation by plasma is inherently multi-mechanistic and arises from the synergistic action of short-lived radicals (e.g., O, OH), long-lived species (e.g., O_3, NO_x), UV photons, and energetic charged particles [4–6]. Previous studies by Fridman et al. [4] and Schmidt et al. [5] have shown that these mechanisms collectively induce oxidative stress, lipid peroxidation, protein denaturation, and irreversible DNA damage, ultimately leading to membrane disruption and cell death. Optical emission spectroscopy (OES) studies by Machala et al. [7] further confirmed the presence of excited nitrogen and oxygen species in air plasmas, providing direct evidence of chemically active environments relevant to biological targets. The relative contribution of each inactivation pathway strongly depends on plasma configuration, operating pressure, power coupling, and spatial proximity to the discharge region.

Among various plasma sources, radio-frequency (RF) capacitively coupled plasma (CCP) systems offer precise control over fundamental plasma parameters such as electron density, electron temperature, sheath dynamics, and ion energy distributions [8]. Although RF CCP discharges are widely employed in materials processing and semiconductor fabrication, their application to biological sterilization, particularly using ambient air as the working gas remains comparatively underexplored. Air-based plasmas offer clear advantages in terms of simplicity, cost-effectiveness, and environmental sustainability by eliminating the need for noble gases or chemical additives [1,9]. However, the complex nitrogen–oxygen chemistry inherent to air plasmas often leads to spatially non-uniform RONS distributions, complicating process optimization and reproducibility.

Low- and medium-pressure air plasmas (1–10 mbar) occupy a transitional regime between atmospheric-pressure discharges and high-vacuum plasma systems. In this pressure range, electron–neutral collision frequencies, reactive species transport, and plasma–surface interaction pathways differ significantly from those observed at atmospheric pressure [8,10,11]. Despite their practical relevance, many plasma sterilization studies lack spatially resolved plasma diagnostics, limiting the ability to directly correlate local plasma properties with microbial inactivation efficiency. As emphasized by Becker et al. [1], understanding the spatial distribution of plasma parameters is essential for optimizing non-equilibrium air plasmas for reliable and scalable sterilization applications.

Early foundational studies on plasma-based microbial inactivation and sterilization, including work by Moisan et al. (2002) [12] and Lerouge et al. (2001) [13], established key mechanistic concepts and demonstrated efficacy of low-temperature plasmas for decontamination. Since then, progress has been driven by improved reactor control and diagnostics, enabling spatially resolved characterization of plasma parameters and more quantitative correlation between discharge structure, reactive pathways, and biological outcomes. The present work contributes to this development by combining 2D Langmuir-probe mapping with spatially resolved inactivation measurements in an air RF CCP at medium pressure.

We therefore clarify that the novelty of the present work is the combined spatial mapping of key plasma parameters (n_e, effective T_e, and V_p) together with spatially resolved inactivation measurements in the same RF CCP air reactor, enabling a direct correlation between discharge structure and strongly localized bacterial inactivation

In this work, bacterial inactivation is investigated using a 13.56 MHz RF capacitively coupled plasma operating in ambient air at a medium pressure of 4.0 mbar. By integrating spatially resolved Langmuir probe diagnostics and optical emission spectroscopy with quantitative microbiological assays, this study systematically examines the relationship between plasma characteristics and sterilization performance. *Escherichia coli* (ATCC 11775)

is employed as a model organism to evaluate inactivation kinetics as a function of RF power, exposure time, and spatial position relative to plasma discharge.

The primary objective of this study is to establish a direct correlation between electron density, electron temperature, reactive species generation, and bacterial log reduction under non-thermal conditions. Particular emphasis is placed on identifying power thresholds and spatial effects governing the transition from partial inactivation to near-complete sterilization. By demonstrating effective and localized microbial inactivation using a gas-free, air-based RF CCP system, this work advances the fundamental understanding of plasma–biological interactions and provides a scalable framework for plasma-assisted sterilization in biomedical and surface decontamination applications.

2. Experimental Setup

2.1. Plasma Generation System

The experiments were carried out in a custom-fabricated cylindrical stainless-steel vacuum chamber with an internal diameter of 30 cm and a length of 20 cm as shown in Figure 1. Two parallel circular electrodes, each 15 cm in diameter, were mounted axially inside the chamber with an inter-electrode spacing of 7 cm. The bottom electrode was powered by a 13.56 MHz radiofrequency (RF) generator, model HF-300 (ENI, Rochester, NY, USA), through a custom-built impedance-matching network fabricated in-house, while the top electrode was electrically grounded, forming a capacitively coupled plasma (CCP) configuration.

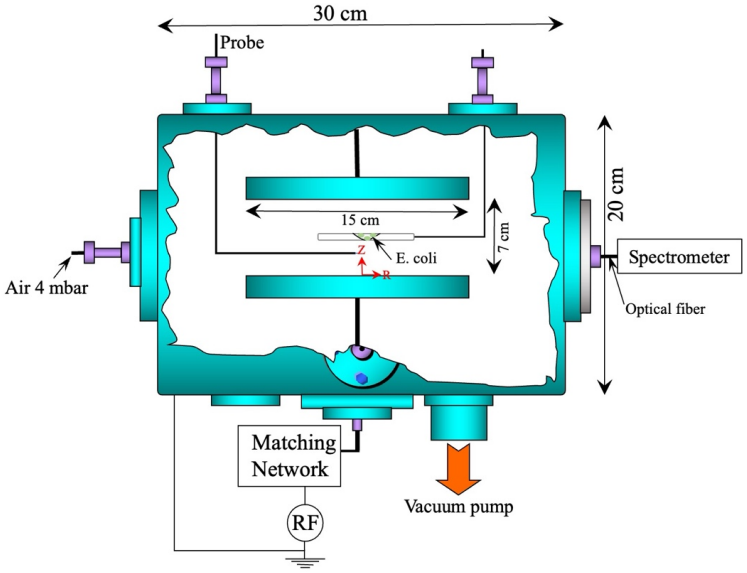


Figure 1. Schematic of the parallel-plate RF capacitively coupled plasma reactor operated in air at 4.0 mbar. The powered electrode (diameter 15 cm) is separated from the grounded electrode by a 7 cm gap inside a 30 cm-long chamber. The coordinate system (*R*,*Z*) is defined with $R = 0$ at the chamber axis and $Z = 0$ at the powered electrode surface (positive Z directed toward the grounded electrode). The Langmuir probe translation path and optical emission spectroscopy (OES) line-of-sight are indicated. Sample positions used for microbiological exposure tests are marked at the discharge center and at peripheral/off-axis locations.

Ambient air was used as the working gas without the addition of external feed gases, emphasizing a gas-free and cost-effective plasma generation approach. The chamber pressure was maintained at 4.0 mbar using a rotary vane vacuum pump (Edwards, Burgess Hill, West Sussex, UK) in conjunction with a needle valve (Edwards, Burgess Hill, West Sussex, UK). This operating pressure corresponds to the medium-pressure regime,

where electron-neutral collision dynamics and reactive species transport differ significantly from both atmospheric-pressure and high-vacuum plasmas, as reported in previous RF CCP studies [1,8]. All experiments were conducted under non-thermal conditions, as verified by in situ temperature measurements presented in Section 3.

2.2. Plasma Diagnostics

2.2.1. Langmuir Probe Measurements

Spatially resolved plasma diagnostics were carried out using a custom-built, in-house fabricated RF-compensated cylindrical Langmuir probe with a silver tip of 0.4 mm diameter and 2 mm length. The probe was introduced through a vacuum-sealed radial port and translated to prescribed locations in both the radial (R) and axial (Z) directions with respect to the powered electrode. At each position, the probe I–V characteristic was acquired over multiple sweeps and averaged to reduce RF-cycle and electronic noise effects.

The plasma potential V_p was obtained from the characteristic "knee" of the I–V curve (equivalently, the inflection point/maximum in dI/dV), while the electron temperature T_e was determined from the slope of the electron-retarding region assuming a locally Maxwellian electron energy distribution. The electron density n_e was calculated from the electron saturation current using the standard cylindrical probe formalism (thin-sheath/orbital-motion considerations as appropriate for the local Debye length and collisionality). The adopted analysis procedure follows established Langmuir probe methodology for low-temperature plasmas [8,14].

Because the discharge is RF-driven and operated in air, the reported parameters represent effective values and carry additional uncertainty near strong sheath regions where RF modulation and electronegativity can distort the I–V curve. These measurements were used to correlate the spatial distributions of n_e, T_e, and V_p with the observed spatial localization of bacterial inactivation.

At the operating pressure of 4.0 mbar (≈400 Pa), probe collection can fall in a weakly collisional regime and the electron energy distribution in air plasmas may deviate from a strictly Maxwellian form. Accordingly, the extracted n_e, T_e, and V_p values are interpreted as effective, locally derived parameters and are used primarily to quantify spatial structure and power trends rather than to reconstruct the full EEDF. Because the discharge is RF-driven and operated in air, additional uncertainty may occur near strong sheath regions where RF modulation and electronegative chemistry can distort the I–V characteristic. Nevertheless, repeated RF-compensated sweeps at representative locations confirmed reproducible I–V characteristics and parameter trends, enabling correlation of the spatial distributions of n_e, T_e, and V_p with the observed spatial localization of bacterial inactivation. A full EEDF reconstruction (e.g., Druyvesteyn analysis) is identified as valuable future work. In electronegative gases such as air, negative ions and attachment processes can modify sheath formation and distort probe characteristics, particularly under RF excitation. The reported parameters are therefore treated as effective values for the adopted method, and detailed electronegative-probe modeling would be required to extract negative-ion densities quantitatively [15,16].

2.2.2. Optical Emission Spectroscopy (OES)

Optical emission spectroscopy (OES) was used to identify excited species produced in the RF air plasma and to track their relative changes with operating conditions. Emission spectra were acquired with a fiber-coupled spectrometer (BWSpec, B&W Tek, Newark, DE, USA) over 200–900 nm. Spectral acquisition was performed using BWSpec, version 4.15 (B&W Tek, Newark, DE, USA). The collection optics viewed the discharge along a fixed line-of-sight at a defined position relative to the electrode gap

(specified in figure captions), and spectra were acquired with an integration time of 200 ms and averaged over 20 scans at each condition. Acquisition settings were kept constant for all RF powers to enable relative intensity comparisons, and care was taken to avoid detector saturation. Spectral features monitored included the O I triplet at 777 nm, the N_2 second positive system (SPS, 337–380 nm), the N_2^+ first negative system (FNS, e.g., near 391 nm when resolved), and hydrogen alpha (Hα, 656 nm).

OES measurements were used qualitatively: emission intensities are reported in relative units (not absolutely calibrated) and therefore indicate changes in excitation/ionization activity and emitting-species populations rather than absolute ground-state RONS concentrations. Absolute quantification (e.g., calibrated radiometry and/or actinometry) is identified as future work.

Air discharges can be sensitive to water vapor (humidity) from the feed gas and desorption from chamber surfaces, particularly with rotary-vane pumping. The observed Hα emission indicates participation of H-containing species and is consistent with H_2O related dissociation/excitation pathways that may support OH-related oxidative chemistry. However, OH emission can be weak and short-lived and may not be readily detected even when chemically important [17]. In this study, humidity/partial pressures were not directly measured (e.g., by residual gas analysis), which is a limitation; future work will include controlled humidity or RGA measurements to quantify its impact on plasma chemistry and inactivation kinetics.

To quantify trends, intensities were background-subtracted and evaluated either as peak intensities or as band-integrated emission over fixed wavelength windows. Because the instrument response was not absolutely calibrated, the reported intensities are relative and should be interpreted as qualitative proxies for changes in excitation and dissociation pathways rather than absolute RONS densities. The dependence of the selected emission features on RF power provides qualitative evidence for increased production of reactive oxygen and nitrogen chemistry and, when combined with the spatially resolved probe diagnostics, supports interpretation of the spatial localization of microbial inactivation.

Data processing, graphing, and figure preparation were carried out using OriginPro, version 19 (OriginLab Corporation, Northampton, MA, USA).

2.3. Bacterial Sample Preparation and Exposure

Aliquots of *Escherichia coli* (ATCC 11775; American Type Culture Collection, Manassas, VA, USA) of 100 µL were deposited onto sterile glass slides placed in Petri dishes (Plasti Lab, El Roumieh, Lebanon) and allowed to dry at 37 °C prior to plasma exposure (dry surface exposure). After treatment, bacteria were recovered by resuspending each slide in 100 µL PBS and homogenizing by vigorous mixing, followed by serial dilution and plating on LB agar for CFU enumeration.

To evaluate spatially resolved inactivation, samples were positioned at three locations:

1. Core discharge region (direct exposure): centered above the powered electrode, where the local plasma density and excitation intensity are maximal.
2. Peripheral/afterglow region: near the chamber wall (off-axis), where the discharge emission is weak and the chemistry is expected to be dominated by longer-lived species transported from the active region.
3. Control: samples kept under identical environmental conditions but not exposed to plasma (outside the active plasma region/plasma off).

Plasma exposures for inactivation assays were performed at RF power of 20–50 W with treatment times in the range 10–600 s (as specified for each experiment). After treatment, surviving bacteria were recovered and quantified by serial dilution followed by standard

plate counting. Colony-forming units (CFUs) were enumerated after incubation, and inactivation was expressed as the $\log_{10}$ reduction:

$$\log_{10} \text{Reduction} = \log_{10}(N_0) - \log_{10}(N_t), \quad (1)$$

where N_0 is the mean CFU count of untreated control samples and N_t is the CFU count after plasma exposure time t. When zero colonies were observed, a half-count correction was applied by assigning 0.5 CFU on the least-diluted plate for log-scale calculations. Each condition was performed in triplicate (n = 3), and results are reported as mean ± SD. When CFU counts were below the assay detection limit, inactivation was reported as ≥ the corresponding $\log_{10}$ reduction (censored at the detection limit).

2.4. Spatial Arrangement

The spatial placement of the sterile slides was designed to enable a direct correlation between local plasma properties and bacterial inactivation. Sample locations were defined in the same (R,Z) coordinate system used for the Langmuir probe mapping, with Z = 0 at the powered RF electrode surface and R = 0 on the chamber axis. Slides were positioned at (i) the core discharge region (on-axis, directly above the powered electrode) and (ii) an off-axis/peripheral region near the chamber wall, where the discharge emission and probe-derived plasma parameters were substantially reduced relative to the core.

Because the measured plasma parameters exhibit pronounced spatial gradients, the two placements provide distinct exposure conditions: the core region corresponds to the zone of strongest coupling and highest measured n_e (and associated excitation), whereas the peripheral placement probes the effect of reduced plasma intensity and transport-dominated chemistry (longer-lived species) on sterilization performance. This spatial arrangement therefore allows the sterilization efficacy to be interpreted in terms of the experimentally determined gradients in n_e, T_e, and V_p, rather than RF power alone.

3. Results and Discussion

3.1. Power-Dependent Plasma Characteristics

Electron Density n_e, and Electron Temperature T_e

Figure 2 shows the dependence of the electron density n_e and electron temperature T_e on the applied RF power, measured on the chamber axis at a fixed axial position Z = 3.5 cm above the powered electrode. As the RF power is increased from 10 W to 100 W, n_e rises monotonically from approximately 6×10^8 cm^{-3} to 3.5×10^9 cm^{-3}. The strong increase in n_e with RF power indicates enhanced electron production via electron-impact ionization, driven by larger oscillatory sheath fields and increased absorbed power in the discharge. Such density scaling with input power is a characteristic feature of RF capacitively coupled plasmas, where higher power increases the ionization source term while particle losses remain dominated by transport to bounding surfaces. This trend is consistent with established CCP behavior and with prior studies reporting electron densities in the 10^8–10^9 cm^{-3} range for air or air-containing RF plasmas at low–medium pressures under comparable conditions [8,18–21].

An increase in n_e implies a higher frequency of electron–molecule collisions and therefore higher rates of excitation, dissociation, and ionization of N_2 and O_2. This, in turn, is expected to enhance the formation of reactive plasma chemistry relevant to sterilization. In the present work, this is supported qualitatively by the observed rise in OES emission features associated with oxygen and nitrogen excitation, which increase with RF power and indicate more active plasma chemistry at higher n_e [4,9,10]. The strong power dependence of n_e also supports the formation of a dense active region in the vicinity of the powered electrode, consistent with the spatial gradients measured in the discharge. Such nonuniform

plasma structures naturally lead to spatially localized reactivity, providing a physics-based explanation for the experimentally observed dependence of bacterial inactivation on sample position (Section 3.2).

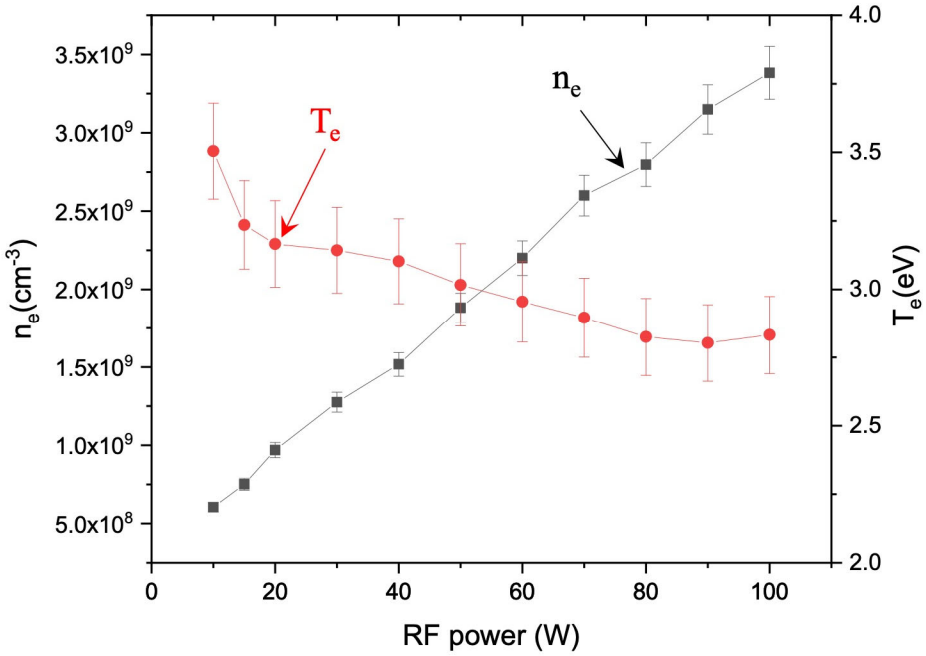


Figure 2. Electron density n_e and electron temperature T_e measured by Langmuir probe as a function of applied RF power (13.56 MHz) for the CCP air discharge at 4.0 mbar. Measurements were taken at a fixed location (R,Z) = (0, 3.5) cm from the powered electrode surface. Error bars represent ± SD obtained from n = 3 independent I–V sweeps. Increasing RF power produces a strong increase in n_e, while T_e varies only weakly over the investigated range, consistent with enhanced ionization at approximately stable effective electron energy.

Figure 2 also presents the dependence of the electron temperature T_e on RF power. A slight but systematic decrease is observed, from approximately 3.51 eV at 10 W to 3.15 eV at 100 W. This weak inverse trend is consistent with collisional low-temperature plasmas in which increasing density enhances the overall rate of inelastic electron energy losses (e.g., vibrational and electronic excitation channels in molecular gases) and promotes redistribution of electron energy through more frequent collisions, resulting in a modest reduction in the effective T_e inferred from the probe analysis [8,14]. Similar behavior strongly increasing density accompanied by a weakly decreasing or nearly constant T_e has been reported in RF plasma systems when operation shifts toward a more strongly sustained, higher-density regime [18,19].

Importantly, the modest decrease in T_e does not imply reduced chemical activity. In molecular gases such as air, electron energies of a few eV remain effective in driving excitation and dissociation processes and sustaining reactive chemistry, particularly when the electron density increases substantially. Thus, the combined trends of increasing n_e and weakly decreasing T_e indicate a plasma regime in which higher absorbed power primarily increases the number of reactive electrons rather than strongly increasing their mean energy, which is consistent with the observed enhancement of emission intensities and the transition to rapid bacterial inactivation at higher RF power.

3.2. Spatial Plasma Profiles

3.2.1. Electron Density Mapping

Figure 3 shows the two-dimensional spatial distribution of the electron density n_e (R,Z) inside the RF CCP chamber at an applied RF power of 50 W (air, 4.0 mbar). The density exhibits a strongly localized maximum of approximately 2×10^9 cm^{-3} near the discharge core, close to the geometric center of the powered electrode at Z = 1.5 cm above the electrode surface. Away from this region, n_e decreases rapidly in both the radial and axial directions, falling to values on the order of 10^8 cm^{-3} toward the chamber periphery and farther from the powered electrode.

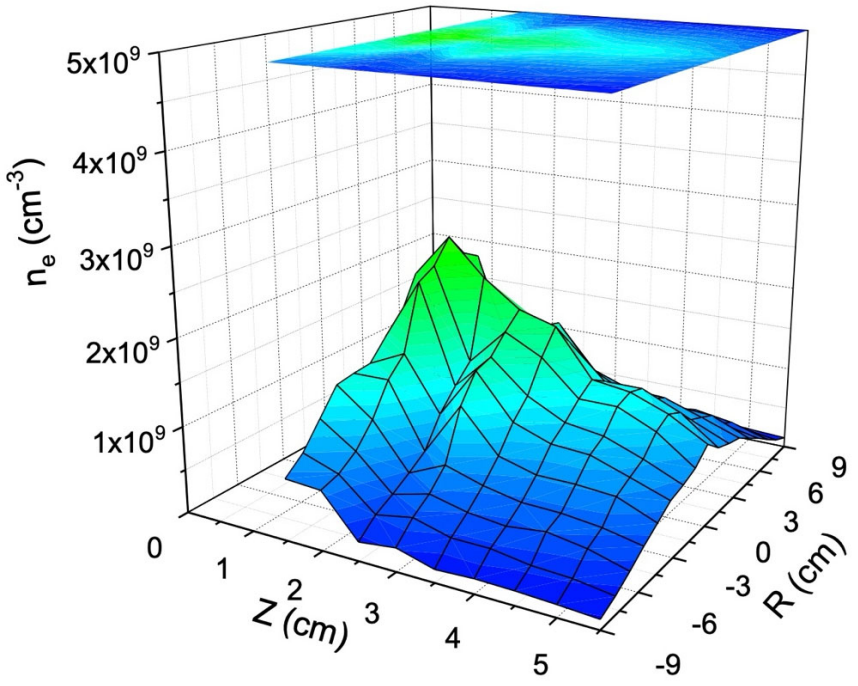


Figure 3. Electron density map n_e (R,Z) measured by RF-compensated Langmuir probe in the RF CCP air discharge (4.0 mbar, 50 W, 13.56 MHz). A localized high-n_e region forms above the powered electrode with strong axial/radial decay; sampling grid: ΔR = 1 cm and ΔZ = 0.5 cm.

This pronounced spatial gradient is characteristic of capacitively coupled RF discharges, in which the dominant energy deposition occurs through the oscillating sheaths adjacent to the electrodes. The sheath expansion and associated RF electric fields drive electron heating most efficiently near the powered electrode region, increasing the local ionization source term and producing a confined high-density core. In addition, the finite electrode radius and proximity of sidewalls introduce radial nonuniformity: enhanced wall-loss area and shorter diffusion paths at larger $|R|$ increase particle losses, so the density must decrease away from the region of strongest power deposition to satisfy the steady-state balance between volumetric production and boundary losses.

The density map also suggests an asymmetric active region and a constriction-like zone. Such features can arise in finite-radius RF CCP systems at moderate pressure due to localized sheath heating, collisional transport, and boundary-driven losses; however, they can also be accentuated by spatial sampling/interpolation and probe-related uncertainty. The structure was reproducible across repeated scans at the same grid spacing, suggesting it reflects a persistent discharge feature, but complementary diagnostics would further validate the detailed morphology.

At the operating pressure of 4.0 mbar, collisional processes further reinforce localization. Frequent electron–neutral collisions reduce electron mean free paths and limit the

spatial spread of energetic electrons, while ion–neutral collisions influence transport to surfaces; together, these effects increase the sensitivity of n_e to local power deposition and boundary conditions. The net result is a discharge with a well-defined active core and strong gradients in plasma parameters across the chamber volume.

The measured n_e (R,Z) profile provides a direct plasma-physics basis for the experimentally observed spatial dependence of bacterial inactivation. Samples placed in or near the high-density core are exposed to the highest rates of electron-driven excitation and dissociation (and therefore the strongest reactive plasma chemistry), whereas samples positioned off-axis or near the chamber wall experience substantially reduced plasma activity. Thus, the density map demonstrates that sterilization performance in this system is governed not only by RF power but also by the spatial distribution of the active plasma region within the reactor.

3.2.2. Electron Temperature Mapping

Figure 4 presents the spatial distribution of the electron temperature T_e (R,Z) measured at 50 W in the RF CCP air discharge (4.0 mbar). Over the mapped region, T_e exhibits a comparatively weak spatial variation, remaining within approximately 5.25–8.17 eV. A modest increase in T_e (R,Z) is observed toward the chamber periphery, whereas slightly lower values occur in the region directly above the powered electrode.

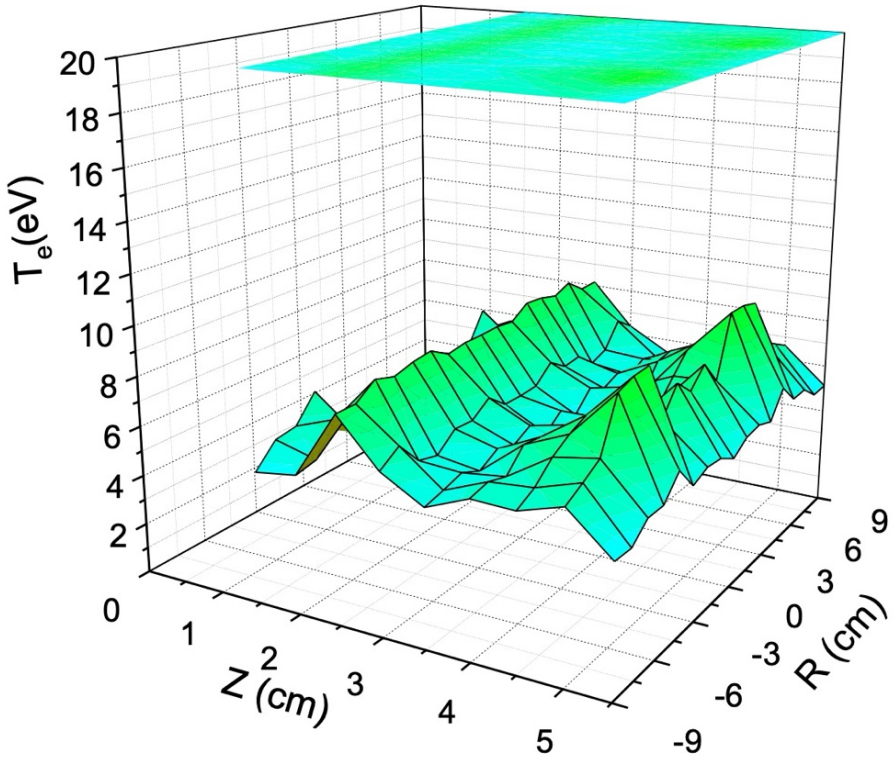


Figure 4. Effective electron temperature T_e (R,Z) extracted from the electron-retarding region of the compensated probe I–V curves under the same conditions as Figure 3. Data are shown as an interpolated contour map with the measurement grid ΔR = 1 cm and ΔZ = 0.5 cm.

A relatively smooth T_e (R,Z) profile is consistent with operation in a collisional molecular plasma, where frequent electron–neutral collisions and energy exchange processes tend to redistribute electron energy and reduce strong spatial contrast in the effective temperature inferred from probe analysis. The slightly elevated T_e values at larger $|R|$ can be attributed to the concurrent reduction in electron density in the periphery (Figure 3), which lowers the rate of collisional energy losses per unit volume and can increase the local mean

electron energy required to sustain the discharge. Conversely, the region above the powered electrode typically supports the highest density and strongest excitation/ionization activity; enhanced inelastic energy loss channels in this zone can produce a modest reduction in the inferred T_e, even while the plasma remains highly reactive.

The absolute T_e values in Figure 4 differ from those extracted in the power-dependence measurements (Figure 2). This difference is expected because Langmuir probe-derived T_e in an RF discharge is sensitive to measurement location, local sheath modulation, and the choice of fitting region in the electron-retarding part of the I–V characteristic. Accordingly, the reported T_e values should be interpreted as effective electron temperatures representative of the local electron energy distribution under the adopted probe analysis procedure [14]. Despite this, the spatial T_e map remains useful because it demonstrates that electron energy and hence the capacity for electron-impact excitation and dissociation does not collapse outside the core region, supporting plasma-driven chemistry across a significant fraction of the chamber volume.

3.2.3. Plasma Potential Mapping

Figure 5 shows the spatial distribution of the plasma potential V_p (R,Z) in the RF CCP air discharge at 50 W and 4.0 mbar. The axial coordinate is defined such that Z = 0 corresponds to the powered RF electrode surface, and Z increases toward the grounded electrode; the radial coordinate spans approximately $R = \pm 9$ cm. The map demonstrates that the discharge is not equipotential: V_p exhibits a structured "basin–ridge" landscape with measurable axial and radial gradients and localized maxima at specific (R,Z) locations. Such spatial variation is physically expected in finite-radius CCP reactors, where power deposition is strongest near the electrode sheath region and where particle transport and wall losses vary across both R and Z.

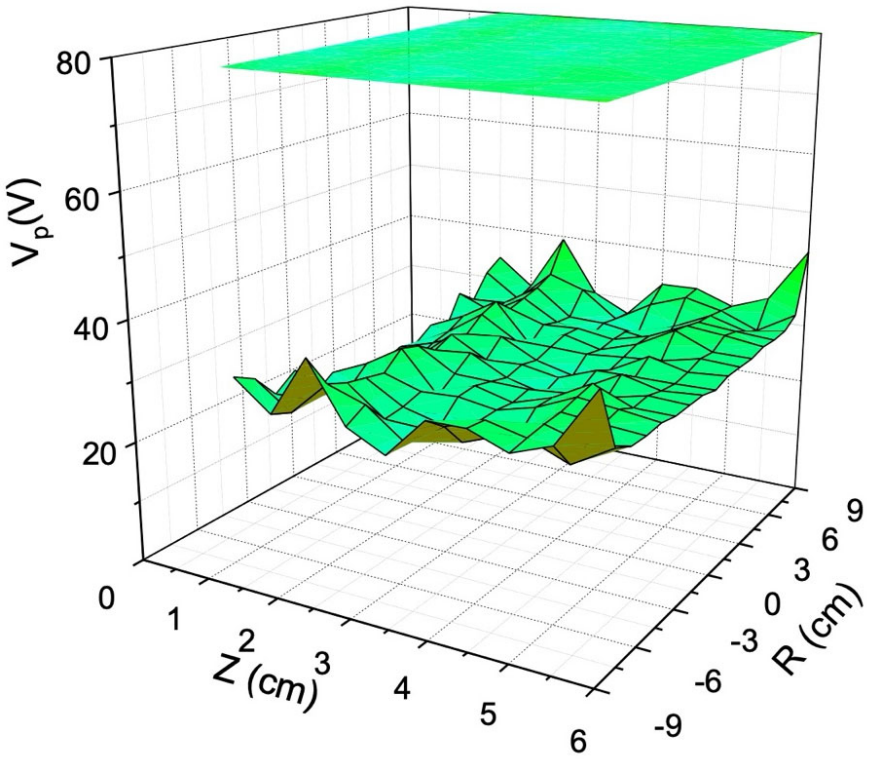


Figure 5. Plasma potential map V_p (R,Z) obtained from compensated Langmuir probe analysis at 4.0 mbar and 50 W. The potential shows measurable axial/radial structure, consistent with spatially varying sheath–bulk coupling and boundary-driven transport losses.

A positive plasma potential is required to confine electrons and maintain global current balance. In steady state, V_p adjusts so that the time-averaged electron losses to boundaries are compatible with ion losses, and it is therefore closely linked to the local electron energy and transport. A standard sheath/flux-balance estimate relates the plasma potential scale to the electron temperature through

$$V_{p-}V_f \approx \frac{T_e}{2e} ln(\frac{m_i}{2\pi m_e}), \quad (2)$$

so spatial structure in the effective electron temperature (or in the electron energy distribution) can manifest as spatial structure in V_p. In addition, when strong density gradients exist (as shown by the n_e (R,Z) map), the plasma establishes an ambipolar field to keep electron and ion transport coupled; consequently, gradients in n_e and T_e naturally lead to gradients in V_p throughout the quasi-neutral region.

The observed axial variation of V_p is particularly relevant in RF CCP operation because the plasma is bounded by two oscillating sheaths. Differences in sheath dynamics between the powered and grounded sides (electrode asymmetry, self-bias formation, and position-dependent electron heating) can produce weak but finite bulk potential gradients to maintain RF current continuity and ambipolar diffusion across the gap. The radial variation reflects finite-size effects: toward larger $|R|$, enhanced wall-loss area and shorter diffusion paths increase particle losses, while edge-field enhancement and sheath curvature modify local heating and sheath–bulk coupling. These combined effects produce the measured nonuniform V_p (R,Z) landscape.

Localized "spikes" in V_p may represent genuine localized regions of enhanced electron heating or sharp gradients in n_e and T_e. However, in RF air plasmas, V_p extracted from probe I–V characteristics can also be sensitive to RF modulation, sheath expansion around the probe, and electronegative chemistry effects. For this reason, the peaks should be interpreted as physical only if they are reproducible under repeated sweeps; overlaying the underlying measurement grid and reporting the uncertainty in V_p extraction are recommended. Possible negative-ion contributions were not resolved as a distinct feature in the present dI/dV-based extraction; consequently, we do not interpret the data as a direct measurement of negative-ion populations [15,16].

In addition to the spatial structure at 50 W, the plasma potential varies only weakly with RF power at the reference position, remaining within a narrow range. This weak power dependence is consistent with CCP scaling in which increasing RF power primarily increases plasma density and ionization rate, while the time-averaged potential structure is constrained by sheath/bulk current balance and stable impedance matching conditions. From the standpoint of plasma-based sterilization, a relatively stable V_p is advantageous because it implies that increases in RF power enhance plasma reactivity mainly by increasing n_e and excitation/dissociation activity, rather than by dramatically increasing ion acceleration energies at the surface.

3.3. Optical Emission Spectroscopy (OES) and Reactive Species Generation

Optical emission spectroscopy (OES) was employed to identify the dominant excited and ionized emitters produced in the RF capacitively coupled plasma (CCP) discharge operated in ambient air at 4.0 mbar and 50 W. A representative spectrum is shown in Figure 6, covering the near-UV/visible/near-IR spectral region accessible to the spectrometer (instrument range stated in Section 2.2.2). The spectrum confirms that the discharge operates in a chemically active, non-equilibrium regime in which electron-impact processes efficiently populate excited states of nitrogen- and oxygen-containing species.

Prominent spectral features were assigned to the N_2 s positive system (SPS, ~337–380 nm), the N_2^+ first negative system (FNS; e.g., near 391 nm when resolved), Hα (656 nm), and

atomic oxygen O I (777 nm). Additional emission in the red/near-IR region is consistent with excited nitrogen/NO-related radiative transitions typically observed in air plasmas containing trace water vapor and complex N_2–O_2 chemistry. The presence of both N_2 SPS and N_2^+ FNS emissions indicates active excitation and ionization pathways driven by electron impact, while the O I (777 nm) line evidence significant oxygen-related excitation/dissociation activity [7,8].

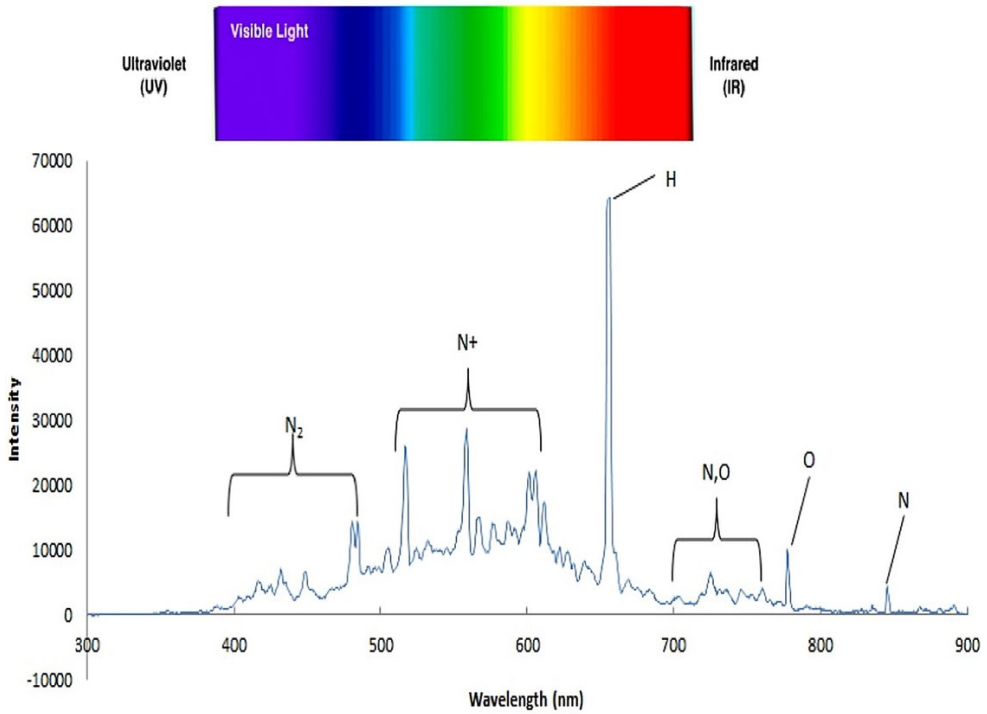


Figure 6. Labeled optical emission spectrum of RF air plasma (13.56 MHz, 50 W, 4.0 mbar), showing key peaks from N_2, N_2^+, Hα, O, and NO species. These emissions indicate the presence of reactive species responsible for bacterial inactivation.

Although OES does not directly quantify ground-state neutral densities, the observed emissions provide qualitative evidence for conditions that favor the generation of biologically relevant reactive oxygen and nitrogen chemistry. Electron-impact dissociation and excitation of O_2 and N_2, together with subsequent gas-phase reactions, are expected to produce reactive species such as O, OH, and NO in the plasma and near-plasma region, while longer-lived species (e.g., O_3, NO_2) can form downstream through post-discharge chemistry depending on residence time and mixing [2,4,10]. These reactive species are widely implicated in plasma-induced microbial inactivation through oxidative and nitrosative stress mechanisms, including membrane lipid oxidation, protein modification, and DNA damage [4,5,22]. In the present work, the systematic strengthening of key emission features with operating power (Figure 7) is consistent with increased excitation/ionization activity and supports the observed enhancement in bacterial inactivation at higher RF power.

Emission features and their biological relevance. The major spectral features observed in the RF air plasma and their relevance to plasma-driven inactivation pathways are summarized in Table 1.

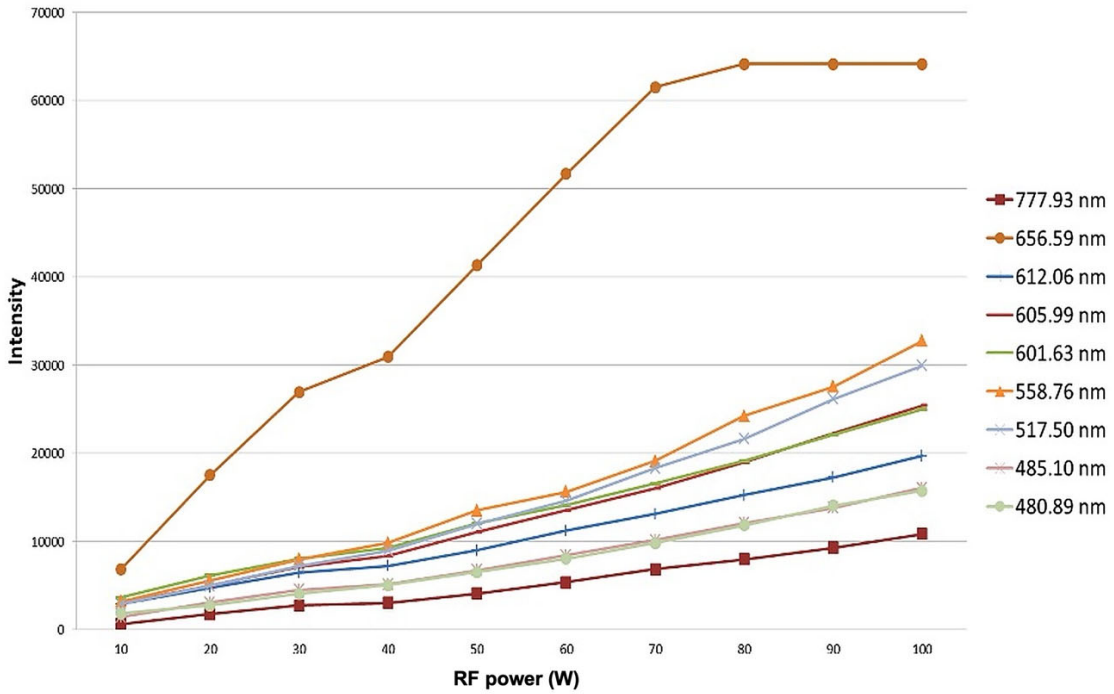


Figure 7. Integrated optical emission intensities of selected spectral features as a function of applied RF power for the RF CCP air discharge at 4.0 mbar (13.56 MHz). Emission was integrated over fixed wavelength windows for each transition/band to quantify relative trends with power; intensities are reported in arbitrary units and are comparable across the power sweep because identical acquisition settings were used. Trends were verified by repeat acquisitions at representative power levels.

Table 1. Major optical emission features observed in the RF CCP air plasma (4.0 mbar) and their qualitative relevance to bacterial inactivation. Emission indicates excited-state populations and is used here as a proxy for discharge excitation/ionization activity rather than a direct measure of ground-state RONS densities.

Emission Line	Species	Wavelength (nm)	Dominant Process	Antimicrobial Relevance	Ref.
N_2 (SPS)	N_2 (C→B)	337–380	Electron-impact excitation	Marker of active electron excitation that supports air-plasma chemistry leading to RONS	[7,10]
N_2^+ (FNS)	N_2^+ (B→X)	391–470	Ionization/high-field excitation	Indicator of stronger discharge conditions; may correlate with enhanced plasma–surface interaction	[5,7,10]
Hα	H (Balmer-α)	656	Trace H_2O/H chemistry	Suggests water-vapor participation; supports possible OH-related oxidative pathways (inferred)	[2,7,10]
Red/near-IR bands	Molecular bands	~700	Molecular excitation/recombination	Qualitative marker of nitrogen–oxygen chemistry (NO_x-related pathways)	[7,10]
O I	Atomic oxygen	777	O_2 dissociation/excitation	Proxy for oxygen-related reactive pathways linked to oxidative stress	[4,7,10]
N I	Atomic nitrogen	~868	N_2 dissociation/excitation	Supports active nitrogen chemistry; potential NO_x precursor pathways (inferred)	[7,10]

The strong emission features from atomic oxygen at 777 nm and the nitrogen molecular systems in the 337–391 nm range indicate an energetic discharge with efficient electron-impact excitation and dissociation processes. In particular, enhanced O I (777 nm) emission is consistent with increased oxygen-related excitation/dissociation activity, which is commonly associated with greater production of oxidative chemistry relevant to antimicrobial action. Likewise, prominent N_2 SPS and N_2^+ FNS emissions reflect active nitrogen excitation/ionization pathways that can support downstream formation of reactive nitrogen chemistry through subsequent gas-phase reactions. These oxygen- and nitrogen-derived reactive pathways are widely implicated in plasma-induced damage to bacterial membranes and intracellular components, including oxidative modification of lipids and biomolecules and, in many systems, nitrosative stress mechanisms [4,10,22].

The observation of N_2^+ emission further suggests that high-field regions and ionization processes are significant in the discharge. While the optical signal itself does not quantify ion flux to the surface, the presence of N_2^+ is often associated with operating conditions that can enhance plasma–surface interactions and contribute to membrane perturbation, particularly for Gram-negative organisms [5]. In addition, the H\alpha line at 656 nm indicates the participation of trace water vapor in the discharge chemistry; this supports the possibility of OH-related reaction pathways (via dissociation and subsequent reactions), which are frequently considered among the most potent oxidative mechanisms in plasma–biomaterial interactions [2,22].

Power dependence of emission features and plasma chemistry

As shown in Figure 7, the integrated intensities of the monitored emission features increase monotonically with RF power, indicating enhanced electron-impact excitation and ionization activity as the discharge is driven harder. This trend is consistent with the corresponding increase in electron density with RF power, since higher n_e increases the frequency of electron–molecule collisions and therefore the rate at which excited radiative states are populated. Similar monotonic increases in emission intensity with applied power are commonly reported in RF CCP discharges, reflecting improved power coupling and higher excitation rates at elevated input power [8,18]. Accordingly, the observed intensity increase with RF power supports a qualitative link between increased discharge excitation activity and enhanced inactivation, but does not by itself provide absolute reactive-species concentrations.

Although OES does not directly provide absolute ground-state RONS densities, the observed strengthening of key oxygen- and nitrogen-related emission features with RF power is consistent with increasingly active plasma chemistry and more intense reactive pathways relevant to microbial inactivation. This interpretation is supported by the biological results: higher RF power produces markedly greater inactivation for samples placed within the discharge core region, with the $\log_{10}$ reduction reaching the assay detection limit ($\geq$2.95-$\log_{10}$) at sufficiently high power. Together, the optical and microbiological results indicate that increasing RF power primarily strengthens the discharge excitation/chemistry environment responsible for bacterial inactivation, rather than simply extending the active region spatially.

Overall, the OES trends demonstrate that the RF CCP operated in ambient air at 4.0 mbar can generate a broad spectrum of oxygen- and nitrogen-based excitation/ionization activity without external gas admixtures. The combination of air-based operation and strong power-dependent excitation is consistent with prior reports of plasma sterilization in air discharges and supports the suitability of the present configuration as a spatially controllable, energy-efficient platform for localized microbial inactivation [9,20,23].

3.4. Plasma-Induced Inactivation of E. coli

3.4.1. Experimental Procedure Summary

Escherichia coli (ATCC 11775) was cultured overnight in 10 mL Luria–Bertani (LB) broth at 37 °C and diluted 10^{-2} in phosphate-buffered saline (PBS, pH 7.2). Aliquots of 100 µL were deposited onto sterile slides placed in Petri dishes and dried at 37 °C prior to plasma exposure. Samples were treated in the RF CCP air plasma at applied powers of 20–50 W and exposure times of 5–600 s. (A higher power condition of 90 W was used only for temperature monitoring to confirm non-thermal operation; see Table 2). Following exposure, bacteria were recovered by resuspending each slide in 100 µL PBS and homogenizing by vigorous mixing. Serial dilutions were prepared, and 100 µL aliquots were plated on LB agar for colony-forming unit (CFU) enumeration after incubation.

Table 2. Temperature measurements during plasma exposure.

Power (W)	Temp at Center (°C)	Temp near RF Electrode (°C)
20	22.8	27.6
40	22.4	25.4
50	22.6	28.6
90	25.0	29.0

Bacterial inactivation was quantified as $\log_{10}$ reduction using Equation (1), $log_{10}(\frac{N_0}{N_t})$, where N_0 is the mean CFU concentration of the untreated control and N_t is the CFU concentration after exposure time t.

Half-count correction for non-detects. The lowest plated dilution was 10^{-2} and the plated volume was 100 µL (0.1 mL). Plates yielding zero colonies were treated as non-detects and handled using a half-count correction by assigning 0.5 CFU on the least-diluted plate for log-scale calculations (i.e., half of the minimum count of 1 CFU), corresponding to an effective floor of $0.5/(0.1 \times 10^{-2}) = 500$ CFU mL^{-1} in the recovered suspension.

3.4.2. Control and Baseline Consistency

Untreated control samples (no plasma exposure) exhibited a consistent bacterial concentration of $N_0 \approx 4.5 \times 10^5$ CFU mL^{-1} ($\log_{10}(N_0) \approx 5.65$) with minimal variability between repeats (SD < 0.05 in log units). The observed fluctuations were within expected statistical/counting uncertainty for plate enumeration, indicating good reproducibility of the culture preparation, deposition, recovery, and plating protocol.

3.4.3. Temperature Distribution

To assess whether thermal effects contributed to inactivation, temperatures were measured at the discharge center and near the RF electrode region for applied powers of 20, 40, 50, and 90 W (Table 2). Across all conditions, measured temperatures remained below 30 °C, indicating that the discharge operated in a non-thermal regime during bacterial exposure.

The small temperature rise observed (a few degrees above ambient) is insufficient to account for rapid bacterial inactivation on its own, supporting the conclusion that inactivation is dominated by plasma-specific mechanisms, including oxidative chemistry (reactive oxygen and nitrogen pathways) and other non-thermal plasma–biological interactions. These observations are consistent with the broader plasma biomedicine literature, where non-thermal air plasmas produce antimicrobial effects primarily through chemically reactive pathways rather than bulk heating [2,4,22].

3.4.4. Effect of Plasma Treatment Time

Figure 8 shows the dependence of *E. coli* survival on plasma exposure time for different RF power levels. At lower powers (20–30 W), the $\log_{10}$ reduction increases progressively with time, indicating slower inactivation kinetics under weaker discharge conditions. In contrast, at higher powers ($\geq$40 W), the reduction rises rapidly and reaches the assay reporting ceiling within approximately 60–120 s at the discharge center. Importantly, under the adopted half-count correction (0 colonies treated as 0.5 CFU on the least-diluted plate), outcomes at the ceiling should be reported as $\geq$2.95-$\log_{10}$ rather than "complete inactivation," because lower survivor levels cannot be quantified by the present CFU protocol.

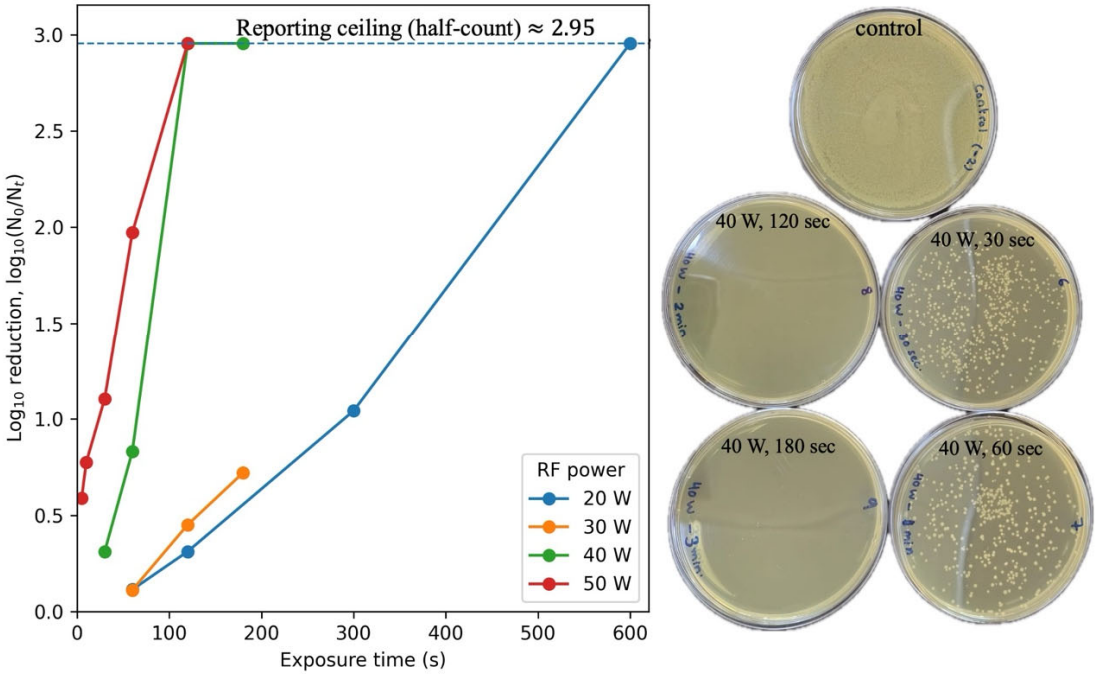


Figure 8. Time-dependent inactivation of *E. coli* (ATCC 11775) in the RF CCP air plasma (4.0 mbar) at 20, 30, 40, 50 W. Samples were placed at the discharge center (on-axis, above the powered electrode) for the power-sweep measurements. Log_{10} reduction is $\text{Log}_{10}(N_0/N_t)$. The dashed line marks the reporting ceiling ($\geq$2.95-$\log_{10}$) under the half-count correction. Representative plates are shown for 40 W RF power.

The time-dependent behavior can be interpreted as three practical regimes:

(i) Regime I: Rapid initial reduction (early-time kinetics)

At short exposure times (typically up to ~60–120 s, depending on power), the log reduction increases steeply, reflecting strong plasma-driven inactivation at the surface. This regime is consistent with immediate plasma–cell interactions dominated by short-lived reactive pathways and other near-surface plasma effects. Because UV emission was not quantified in the present study, we do not attribute early-time kinetics to UV specifically and instead describe this as a rapid initial inactivation phase dominated by plasma-specific near-surface interactions. Quantitative UV radiometry through a UV-transparent viewport is identified as useful future work to assess photon contributions as a function of RF power.

(ii) Regime II: Slower continued inactivation (tailing behavior)

At longer exposure times, the slope of the curve decreases (most evident at lower powers), producing a "tailing" region frequently observed in microbial inactivation studies. Several factors can contribute to this slower apparent rate: heterogeneous exposure on the slide (micro-shielding), survivor subpopulations with higher resistance, and/or reduced accessibility of reactive chemistry to cells protected within aggregates or surface microfeatures.

In this regime, cumulative oxidative/nitrosative stress is expected to continue damaging membranes and biomolecules, but the kinetics can deviate from simple first-order behavior, so linear "*D*-value" interpretations should be applied cautiously and only to the strictly log-linear region (if present).

(iii) Regime III: Reporting-ceiling plateau (censored outcomes)

For sufficiently high power and/or long exposure, the log reduction reaches approximately 2.95-$\log_{10}$, corresponding to the effective floor of 500 CFU mL^{-1} introduced by the half-count correction. Beyond this point, additional inactivation cannot be resolved by the current assay sensitivity, and the appropriate interpretation is censoring: the reduction is at least $\geq$2.95-$\log_{10}$, but the true value may be larger. Accordingly, this region should be described as a detection/quantification-limit plateau rather than "complete sterilization".

Overall, the acceleration of inactivation kinetics with RF power is consistent with the plasma diagnostics: increasing power increases n_e and strengthens excitation/ionization activity (OES trends), which enhances reactive plasma chemistry in the core region where samples experience the highest plasma intensity. The observed time-dependent regimes are consistent with multi-stage, non-thermal plasma inactivation behavior widely reported in the plasma biomedicine literature [2,4,10,22].

3.4.5. Effect of RF Power

Figure 9 shows the effect of RF power on *E. coli* inactivation for a fixed exposure time of 60 s at the discharge center. The $\log_{10}$ reduction increases nonlinearly with increasing RF power, with modest reductions at low power (20–30 W) and a marked rise at higher power ($\geq$40 W), approaching the assay reporting ceiling under the adopted half-count correction (i.e., $\geq$2.95-$\log_{10}$). This strong power dependence is consistent with the plasma diagnostics: increasing RF power increases the electron density n_e and strengthens excitation/ionization activity (OES trends), thereby enhancing the electron-driven pathways that generate biologically active plasma chemistry in air.

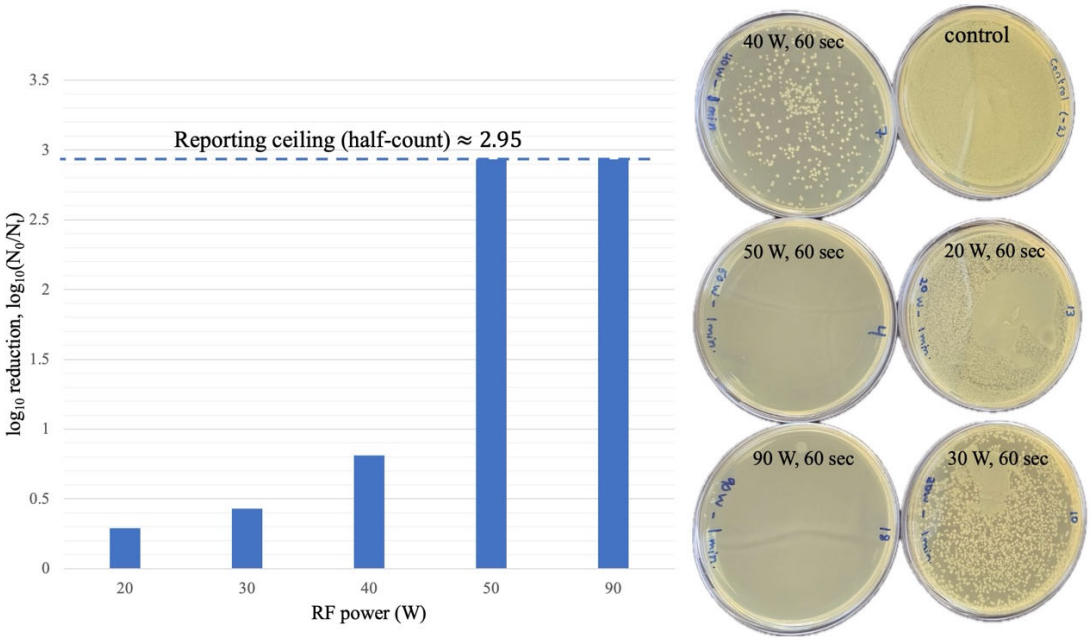


Figure 9. Log_{10} reduction of *E. coli* after 60 s exposure versus RF power in the RF CCP air plasma (4.0 mbar). Representative plates are shown for selected powers; reductions at high power reach the reporting ceiling ($\geq$2.95-$\log_{10}$) under the half-count correction.

At low RF power, the discharge is comparatively weak and the inactivation at 60 s remains limited, consistent with reduced n_e and lower excitation intensity. With increasing power, the rise in n_e implies higher electron–molecule collision frequencies and higher rates of excitation/dissociation processes in N_2/O_2, which increases the overall oxidative/nitrosative reactivity of the plasma environment. At 50 W, the inactivation reaches the reporting ceiling within 60 s, indicating a critical operating regime above which the discharge produces sufficiently intense reactive pathways to drive rapid loss of viability under the present conditions.

The apparent "threshold-like" transition with RF power is physically plausible for CCP operation: modest increases in RF power can shift the discharge toward a higher-density, more strongly sustained regime (higher n_e with only weak changes in effective T_e), producing a disproportionate increase in reactive chemistry and surface interaction intensity in the plasma core region. Similar power-accelerated inactivation behavior has been reported for low-pressure plasma treatments of bacteria, where increased discharge intensity enhances reactive pathways while gas temperature remains low [22]. Overall, the power dependence confirms that RF power is an effective control parameter for tuning the discharge into a regime of rapid bacterial inactivation, with strong dependence on sample placement relative to the active plasma core.

3.4.6. Effect of Spatial Position

Bacterial inactivation was strongly dependent on sample location within the chamber. Samples positioned in the core discharge region above the powered electrode exhibited the largest reductions, whereas samples placed near the chamber periphery/off-axis region showed negligible inactivation $\log_{10}$ reduction $\approx$0 within counting uncertainty) under otherwise identical treatment conditions. This pronounced spatial localization indicates that sterilization efficacy is governed by the local discharge intensity rather than RF power alone.

This spatial trend is consistent with the plasma diagnostics. The measured n_e (R,Z) distribution reveals a confined high-density region near the powered electrode with rapid decay toward the periphery, implying that electron-driven excitation/dissociation pathways and therefore reactive plasma chemistry are concentrated near the discharge core. In addition, the structured V_p (R,Z) landscape indicates nonuniform sheath–bulk coupling and transport fields, which can further localize plasma surface interaction intensity. Together, these results provide a physical basis for why peripheral samples experience substantially weaker plasma exposure: outside the active core, reduced density and excitation activity limit the generation and delivery of biologically relevant reactive pathways to the surface. Such spatial non-uniformity is characteristic of finite-radius CCP systems and has been reported in spatially resolved studies of plasma–biological interactions [2,4,10].

While the present work compares core and peripheral locations to demonstrate strong spatial localization, a full 2D inactivation map over (R,z) aligned with the probe grid would be a valuable extension in future work.

3.4.7. Survival Curves and *D* Values

Survival curves were constructed from CFU measurements by plotting $log_{10}(\frac{N_0}{N_t})$, (or equivalently $\log_{10}$ reduction) as a function of exposure time for each RF power (Figure 8). The corresponding mean $\log_{10}$ reductions at different RF powers and exposure times are summarized in Table 3. To quantify early-time kinetics, D-values (decimal reduction times) were extracted by least-squares fitting of the earliest non-censored portion of each survival curve according to:

$$log_{10}(\frac{N_0}{N_t}) = -\frac{t}{D} \quad (3)$$

Table 3. Mean $\log_{10}$ reduction (mean ± SD, n = 3) of *E. coli* at different RF powers and exposure times. Values at the reporting ceiling are reported as ≥2.95 due to half-count correction (0 colonies treated as 0.5 CFU on the least-diluted plate).

Power (W)	Exposure Time (s)	Mean Log Reduction	SD	Observation
20	60	0.29	0.02	Slow early inactivation
20	120	0.29	0.03	No significant additional reduction
20	300	1.02	0.05	Continued inactivation (tailing)
20	600	≥2.95	0.08	Reached reporting ceiling
30	60	0.43	0.04	Faster early inactivation than 20 W
30	120	0.43	0.03	Limited additional reduction
30	180	0.70	0.05	Continued inactivation
40	30	0.81	0.06	Rapid early inactivation
40	60	0.81	0.05	Near-plateau behavior
40	120	≥2.95	0.07	Reached reporting ceiling
50	5	0.75	0.04	Rapid onset
50	10	0.75	0.03	Rapid onset
50	30	1.08	0.06	Strong increase with time
50	60	≥2.95	0.05	Reached reporting ceiling

Because CFU enumeration is subject to a reporting ceiling under the adopted half-count correction (0 colonies treated as 0.5 CFU on the least-diluted plate), data points that reached the ceiling (≥2.95-$\log_{10}$) were treated as censored and were excluded from the fitting procedure. The resulting *D*-values (Table 4) therefore represent effective early-time inactivation rates within the measurable region of each curve.

Table 4. *D*-values extracted from the earliest non-censored (pre-plateau) log-linear region of the survival curves. Fits exclude censored points at the reporting ceiling (≥2.95).

Power (W)	Fit Window (s)	Points	*D*-Value (s)	R^2
20	60–300	3	255.8	0.998
30	60–180	3	197.4	0.996
40	30–60	2	57.8	1.000
50	5–30	3	51.3	0.970

As summarized in Table 4, *D*-values decrease strongly with increasing RF power, from approximately 256 s at 20 W to ~51 s at 50 W, indicating a substantial acceleration of inactivation kinetics under stronger discharge conditions. This trend is consistent with the plasma diagnostics, where increasing RF power increases electron density and excitation activity, thereby strengthening plasma-driven reactive pathways at the sample surface. Deviations from ideal single-slope behavior (e.g., tailing prior to censoring) are consistent with heterogeneous exposure and shielding effects commonly observed in microbial inactivation studies and do not alter the conclusion that RF power strongly controls the early-time inactivation rate.

3.4.8. Discussion

The plasma-induced inactivation of *E. coli* observed in this study exhibits clear dependence on treatment time, RF power, and sample position, reflecting the spatially structured

nature of the RF CCP discharge and the multi-pathway character of non-thermal plasma sterilization under low gas-temperature conditions.

Time-Dependent Inactivation:

At low RF powers (20–30 W), short exposure times ($\leq$120 s) produced modest reductions ($\approx$0.29–0.43 $\log_{10}$), indicating relatively slow early-time kinetics under weaker discharge conditions. With increasing exposure time, reductions increased progressively, consistent with cumulative plasma-driven effects at the surface and continued exposure to reactive plasma chemistry. At higher powers ($\geq$40 W), reductions increased much more rapidly and reached the assay reporting ceiling within 60–120 s at the discharge center. Under the adopted half-count correction (0 colonies treated as 0.5 CFU on the least-diluted plate), such outcomes should be reported as $\geq$2.95-$\log_{10}$ rather than as absolute sterility, since survivor levels below the reporting floor cannot be quantified with the current CFU protocol.

Power-Dependent Enhancement:

Increasing RF power substantially accelerates bacterial inactivation, consistent with the plasma diagnostics: n_e increases strongly with power while OES emission features associated with nitrogen and oxygen excitation intensify, indicating enhanced excitation/ionization activity and therefore stronger plasma-driven chemical pathways. The sharp rise in inactivation between lower and higher power levels (Figure 9) suggests a transition to a more effective operating regime, where the discharge produces sufficiently intense reactive pathways to rapidly reduce viable counts to the reporting ceiling within 60 s at 50 W. This transition can be interpreted physically as a shift toward a higher-density, more strongly sustained CCP regime, in which increased electron–molecule collision frequency enhances dissociation/excitation and increases the flux of chemically active species to the surface [9,20,23].

Spatial Effects:

A central finding is that bactericidal efficacy is strongly localized to the discharge core above the powered electrode. Peripheral/off-axis samples exhibited negligible reduction ($\approx$0 $\log_{10}$), demonstrating that sterilization performance is governed by local discharge intensity rather than RF power alone. This spatial dependence directly correlates with the measured plasma structure: n_e (R,Z) exhibits a confined high-density region near the powered electrode with strong axial/radial gradients, and the V_p (R,Z) profile indicates nonuniform sheath–bulk coupling and transport fields. Together, these diagnostics provide a physical basis for localized inactivation and demonstrate that sample placement relative to the active plasma region is a critical design parameter for achieving reliable sterilization [2,4,10].

Mechanistic interpretation:

The non-thermal temperature measurements (<30 °C) exclude bulk heating as the primary driver. The observed power dependence of n_e and OES excitation features supports a mechanism dominated by plasma-driven oxidative and nitrosative pathways, consistent with the established plasma biomedicine literature [4,10,22]. While OES does not directly quantify ground-state RONS densities, the presence and strengthening of oxygen- and nitrogen-related emission features with power indicate conditions favorable for generating reactive chemistry in air plasmas. These pathways can induce membrane oxidation and biomolecule damage leading to loss of viability. Additional contributions from photons and charged-particle effects are possible; however, quantifying UV dose and long-lived species would require dedicated measurements and is identified as future work.

The present results demonstrate a strong spatial correlation between discharge intensity (high n_e and enhanced emission features) and inactivation in the plasma core. While this supports oxidative/nitrosative pathways as a highly plausible mechanism, the present study does not isolate individual reactive channels. Cause-and-effect attribution to specific radicals would benefit from targeted control experiments (e.g., chemical scavengers or controlled gas-phase chemistry), which are identified as future work also.

Kinetic metrics and reproducibility:

D-values extracted from the earliest non-censored region of the survival curves (Table 4) decrease strongly with power, from approximately 256 s at 20 W to ~51 s at 50 W, confirming power-accelerated early-time inactivation kinetics. These values fall within the broad range reported for low-temperature plasma bacterial inactivation studies under non-thermal conditions. Finally, the low variability across triplicate measurements (SD < 0.1 $\log_{10}$ in Table 3) supports the robustness and repeatability of the experimental protocol, while the consistent spatial trend (core $\gg$ periphery) confirms that the observed localization is a reproducible property of the discharge structure [20,22]

D-values decrease sharply with RF power, consistent with accelerated early-time inactivation kinetics under stronger discharge conditions.

4. Conclusions

This study demonstrates effective and spatially localized inactivation of *Escherichia coli* using a 13.56 MHz radio-frequency capacitively coupled plasma (RF CCP) operated in ambient air at 4.0 mbar. By combining spatially resolved plasma diagnostics with quantitative microbiological assays, we establish a direct link between discharge structure, excitation/chemistry activity, and bacterial inactivation.

Langmuir probe measurements showed that the electron density n_e increases strongly with RF power, reaching the order of 10^9 cm^{-3} near the powered electrode and exhibiting pronounced axial and radial gradients across the discharge volume. Optical emission spectroscopy revealed a chemically active air plasma characterized by dominant nitrogen molecular emissions (N_2 SPS and N_2^+ FNS) and atomic oxygen emission (O I 777 nm), with emission intensities increasing monotonically with applied power. While OES provides qualitative information on excited-state populations rather than absolute ground-state densities, the observed power-dependent emission trends are consistent with enhanced excitation/ionization activity and increasingly active plasma chemistry at higher RF power.

Microbiological measurements demonstrated clear power- and time-dependent inactivation kinetics. At lower powers (20–30 W), reductions were modest and progressed gradually with exposure time. At higher powers ($\geq$40 W), inactivation accelerated markedly, and at 50 W the reduction reached the assay reporting ceiling within 60 s (reported as $\geq$2.95-$\log_{10}$ under the adopted half-count correction). Time-resolved measurements at 50 W showed that measurable reductions occur within the first seconds of exposure, consistent with rapid early-time kinetics. Importantly, samples positioned outside the discharge core exhibited negligible inactivation, confirming that bactericidal efficacy is strongly localized and governed by the spatial distribution of the active plasma region.

Temperature measurements remained below 30 °C for all investigated powers, confirming non-thermal operating conditions and excluding bulk heating as a dominant contributor. Overall, the results identify RF power and sample placement as key control parameters: increasing power strengthens discharge intensity and plasma chemistry in the core region, while the strong spatial gradients in n_e and potential structure confine effective inactivation to a limited zone above the powered electrode.

These findings establish medium pressure, air-based RF CCP as an efficient, gas-free, and spatially controllable platform for localized surface decontamination. The combined

plasma biological approach provides a scalable framework for optimizing reactor design and operating conditions for nonthermal sterilization applications where spatial selectivity is required.

Author Contributions: Conceptualization, M.N.; methodology, M.N. and L.N.; plasma diagnostics, M.N.; microbiological experiments, F.M. and B.A.; data analysis, M.N. and E.N.; writing—original draft preparation, M.N.; writing—review and editing, all authors; supervision, M.N. All authors have read and agreed to the published version of the manuscript.

Funding: This research received no external funding.

Institutional Review Board Statement: Not applicable.

Informed Consent Statement: Not applicable.

Data Availability Statement: The data presented in this study are available from the corresponding author upon reasonable request.

Acknowledgments: The authors would like to acknowledge the support of the Department of Physics, and Department of biology, University of Bahrain.

Conflicts of Interest: The authors declare no conflicts of interest.

References

1. Becker, K.H.; Kogelschatz, U.; Schoenbach, K.H.; Barker, R.J. Non-equilibrium air plasmas at atmospheric pressure. *IEEE Trans. Plasma Sci.* **2001**, *29*, 41–50.
2. Graves, D.B. Low temperature plasma biomedicine: A tutorial review. *Phys. Plasmas* **2014**, *21*, 080901. [CrossRef]
3. Weltmann, K.-D.; von Woedtke, T. Plasma medicine—Current state of research and medical application. *Plasma Phys. Control. Fusion* **2017**, *59*, 014031. [CrossRef]
4. Fridman, K.; Chirokov, A.; Gutsol, A. Applied plasma medicine: Mechanisms of microbial destruction. *Plasma Process. Polym.* **2008**, *5*, 503–533. [CrossRef]
5. Schmidt, A.; von Woedtke, J.; Weltmann, K.D.; Bekeschus, S. YAP/TAZ, beta-catenin, and TGFb pathway activation in medical plasma-induced wound healing in diabetic mice. *J. Adv. Res.* **2025**, *72*, 387–400. [CrossRef]
6. Naïtali, M.; Kamgang-Youbi, G.; Herry, J.-M.; Bellon-Fontaine, M.-N.; Brisset, J.-L. Combined effects of long-living chemical species during microbial inactivation using atmospheric plasma-treated water. *Appl. Environ. Microbiol.* **2010**, *76*, 7662–7664. [CrossRef]
7. Machala, Z.; Janda, M.; Hensel, K.; Jedlovský, I.; Leštinská, L.; Foltin, V.; Martišovitš, V.; Morvová, M. Emission spectroscopy of atmospheric pressure plasmas for bio-medical and environmental applications. *J. Mol. Spectrosc.* **2007**, *243*, 194–201. [CrossRef]
8. Lieberman, M.A.; Lichtenberg, A.J. *Principles of Plasma Discharges and Materials Processing*, 2nd ed.; Wiley-Interscience: Hoboken, NJ, USA, 2005.
9. Li, Q.; Li, Y.; Liu, H.; Zhang, X. Surface sterilization using RF discharges in ambient air. *Appl. Surf. Sci.* **2022**, *586*, 152742. [CrossRef]
10. Lu, X.; Laroussi, M.; Puech, V. Reactive species in non-equilibrium atmospheric-pressure plasmas: Generation, transport, and biological effects. *Phys. Rep.* **2016**, *630*, 1–84. [CrossRef]
11. Bruggeman, P.; Kushner, M.J. Fundamentals of cold atmospheric pressure plasma technology for biomedical applications. *J. Phys. D Appl. Phys.* **2016**, *49*, 293001. [CrossRef]
12. Moisan, M.; Barbeau, J.; Crevier, M.-C.; Pelletier, J.; Philip, N.; Saoudi, B. Plasma sterilization. Methods and mechanisms. *Pure Appl. Chem.* **2002**, *74*, 349–358. [CrossRef]
13. Lerouge, S.; Wertheimer, M.R.; Yahia, L. Plasma sterilization: A review of parameters, mechanisms, and limitations. *Plasmas Polym.* **2001**, *6*, 175–188. [CrossRef]
14. Chen, F.F. Langmuir probe analysis for high-density plasmas. *Phys. Plasmas* **2001**, *8*, 3029–3041. [CrossRef]
15. Zhou, C.; Wang, H.; Saifutdinov, A.; Saifutdinova, A.; Yao, J.; Nie, Q.; Zhou, Z.; Yuan, C. Is it possible to dynamical monitoring the products of silane conversion in plasma with non-local characteristics using probe diagnostics? *Plasma Sources Sci. Technol.* **2026**, *35*, 025029. [CrossRef]
16. Godyak, V.A.; Demidov, V.I. Probe measurements of electron-energy distributions in plasmas: What can we measure and how can we achieve reliable results? *J. Phys. D Appl. Phys.* **2011**, *44*, 233001. [CrossRef]

17. Rupper, P.; Amberg, M.; Hegemann, D.; Heuberger, M. Optimization of mica surface hydroxylation in water vapor plasma monitored by optical emission spectroscopy. *Appl. Surf. Sci.* **2020**, *509*, 145362. [CrossRef]
18. Zhang, A.; Lee, M.-Y.; Lee, H.-W.; Moon, H.-J.; Chung, C.-W. Effects of RF bias frequency and power on plasma parameters and ash rate in a remote plasma source. *Plasma Sources Sci. Technol.* **2021**, *30*, 025009. [CrossRef]
19. Lee, H.-C.; Lee, M.-H.; Chung, C.-W. Effects of rf-bias power on plasma parameters in a low gas pressure inductively coupled plasma. *Appl. Phys. Lett.* **2010**, *96*, 071501. [CrossRef]
20. von Keudell, A.; Awakowicz, P.; Benedikt, J.; Raballand, V.; Yanguas-Gil, A.; Opretzka, J.; Flötgen, C.; Reuter, R.; Byelykh, L.; Halfmann, H.; et al. Inactivation of Bacteria and Biomolecules by Low-Pressure Plasma Discharges. *Plasma Process. Polym.* **2010**, *7*, 327–352. [CrossRef]
21. Sureshkumar; Neogi, S. Inactivation characteristics of bacteria in capacitively coupled argon plasma. *IEEE Trans. Plasma Sci.* **2009**, *37*, 2347–2352. [CrossRef]
22. Ahmed, M.W.; Naqvi, S.M.; Qasim, I.; Noreen, Z.; Shafiq, M.; Bukhari, H. Degradation of multidrug-resistant *E. coli* by low pressure plasma. *Int. J. Food Prop.* **2021**, *24*, 1289–1299. [CrossRef]
23. Vassallo, E.; Pedroni, M.; Aloisio, M.; Silvetti, T.; Morandi, S.; Brasca, M. Synergistic Action of Reactive Plasma Particles and UV Radiation to Inactivate Staphylococcus Aureus. *Coatings* **2022**, *12*, 1105. [CrossRef]

Disclaimer/Publisher's Note: The statements, opinions and data contained in all publications are solely those of the individual author(s) and contributor(s) and not of MDPI and/or the editor(s). MDPI and/or the editor(s) disclaim responsibility for any injury to people or property resulting from any ideas, methods, instructions or products referred to in the content.